Delivered at the International Conference on Materials for Advanced Technologies 2003, Singapore, December 7−12, 2003

Design of Potential Hydrogen-Storage Materials Using First-Principle Density-Functional Calculations

P. Vajeeston,* P. Ravindran, R. Vidya, H. Fjellvåg, and A. Kjekshus

Department of Chemistry, University of Oslo, Box 1033 Blindern, N-0315 Oslo, Norway

ABSTRACT: The crystal and electronic structures of the entire series of alkali aluminum and alkali gallium tetrahydrides (ABH_4; A = Li, Na, K, Rb, or Cs; B = Al or Ga) are systematically investigated using an ab initio projected augmented plane-wave method. For structural stability studies, we have considered several possible structural modifications, and reproduced successfully the equilibrium structures for the known phases $LiAlH_4$, $NaAlH_4$, $KAlH_4$, $NaGaH_4$, and $KGaH_4$. Moreover, we predict the equilibrium structures of the other unknown members of this series. $RbAlH_4$, $CsAlH_4$, $RbGaH_4$, and $CsGaH_4$ should crystallize with the $KGaH_4$-type structure, and $LiGaH_4$ should crystallize with the $NaGaH_4$-type structure. According to the density of states, all these compounds have nonmetallic character with a finite band gap of around 5 eV. Charge-density plot and electron localization function analyses show that the $[BH_4]$ subunits almost look like a separate molecular species spread over the A matrix. An ionic type of interaction is present between the A and the $[BH_4]$ units. Crystal orbital Hamilton population analyses reveal that the interaction between the B and H atoms is stronger than the other interactions present in these compounds.

Introduction

Prediction and understanding of properties of materials (encompassing even not yet synthesized phases) by theoretical means is a valuable complement to the traditional empirical approach. Theoretical simulation of material properties before preparation and testing may save time, manpower, running costs, etc. Owing to the low X-ray scattering power of hydrogen, poor crystallinity, and the usual structural complexity of hydrides, these structures are often less characterized than other solids.[1] For instance, this is the case for the (assumed technologically interesting materials) alkali aluminum and alkali gallium tetrahydrides among which only $NaAlH_4$, $LiAlH_4$, $NaGaH_4$, and $KGaH_4$ are structurally well characterized. Unit-cell volumes only are available for $KAlH_4$ and $LiGaH_4$ and virtually no structural information exists for ABH_4 with A = Rb and Cs and B = Al and Ga. This type of compound is widely considered to be used for hydrogen storage and preparatives purposes in inorganic and organic chemistry.

A reversible process with storage of hydrogen in the form of an intermetallic hydride has several advantages over the use of conventional pressurized gas cylinders and liquid tanks.[2,3] One of the major drawbacks of all metal hydrides hitherto considered for hydrogen storage in comparison to liquid hydrogen is the low mass of stored hydrogen relative to the mass of the metal hydrides. Magnesium dihydride (with 7.6 wt % stored hydrogen) represents a now prevailing optimum, but for

its use as a storage material heating above 300 °C is necessary for the desorption of hydrogen. The presently most considered so-called low-and high-temperature reversible hydrides have 4−5 times lower storage capacity than MgH_2 as well as high costs.

In view of their high molar content of hydrogen, complex hydrides of light metals such as Li, Na, K, and Al have recently been in the spotlight for hydrogen storage. In 1997, $NaAlH_4$ was introduced as a lightweight reversible hydrogen storage material by Bogdanovic and Schwickardi.[4] The advanced reaction mechanism for formation/decomposition of aluminohydrides is based on reversible steps, in which all constituents migrate. This is significantly different from the reaction mechanisms for conventional metal hydrides in which hydrogen atoms use interstitial crystallographic sites and are the only mobile species. The thermal decomposition of $AAlH_4$ (A = Li, Na, or K) involves three steps:[4−10]

$$3AAlH_4 \rightarrow A_3AlH_6 + 2Al + 3H_2 \qquad (1)$$

$$A_3AlH_6 \rightarrow 3AH + Al + 3/2H_2 \qquad (2)$$

$$3AH \rightarrow 2A + 3/2H_2 \qquad (3)$$
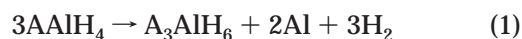
In step I (at ∼112, 33, and 300 °C for A = Li, Na, and K, respectively[7−10]), $AAlH_4$ decomposes into A_3AlH_6, during which 5.3 to 2.9 wt % H is released. In step II (at ∼127, 130, and 340 °C for A = Li, Na, and K, respectively[7−10]), A_3AlH_6 decomposes into AH and Al, further releasing 2.6 to 1.4 wt % of H. Because of the strong bonding interaction between A and H the hydro-

* To whom correspondence should be addressed. E-mail: ponniahv@kjemi.uio.no; URL: http://folk.uio.no/ponniahv.

gen in step III is not available for practical utilization. Recent experimental evidence shows that the releasing of hydrogen from $KAlH_4$ proceeds smoothly without the assistance of a catalyst.[10] This degradation reaction is accordingly markedly different from the decomposition of $NaAlH_4$ and $LiAlH_4$, where homogeneous doping with a transition metal catalyst is essential for the progression of eqs 1 and 2 with good kinetics.[4] To get more insight into the properties of these systems, improved structural information is needed, and the present study is aimed at the crystal and electronic structures of ABH_4; A = Li, Na, K, Rb, or Cs; B = Al or Ga at ambient pressure.

Computational Details

To predict the ground-state crystal and electronic structures, we have used density-functional theory (DFT)[11] within the generalized-gradient approximation (GGA),[12] as implemented with a plane-wave basis in the Vienna ab initio simulations package (VASP).[13] Results are obtained using projected-augmented wave (PAW)[14] potential provided with VASP. The PAW potentials explicitly treat one valence electrons for H ($1s^1$), Li ($2s^1$), and Na ($3s^1$), seven for K ($3p^6$, $4s^1$) and Rb ($4p^6$, $5s^1$), nine for Cs ($5s^2$, $5p^6$, $6s^1$), and three for Al ($3s^2$, $3p^1$) and Ga ($4s^2$, $4p^1$). The ions are steadily relaxed toward equilibrium until the Hellmann−Feynman forces are less than 10^{-3} eV/Å during all relaxations. Experimentally established structural data were used as input for the calculations when available. For the tetragonal $NaAlH_4$, structure we used 432 **k** points in the whole Brillouin zone. A similar density of **k** points was used for the other structures. To avoid ambiguities regarding the free-energy results, we have used the same energy cutoff and similar **k**-grid densities in all calculations. At least 0.01 meV/atom was placed as a criterion on the self-consistent convergence of the total energy, and the calculations reported here used a plane wave cutoff of 500 eV. A similar approach was successfully applied for the case of MgH_2, where the three experimentally observed high-pressure phases were reproduced successfully and two additional high-pressure phases were predicted.[15] To identify the bond strength, we have used the crystal orbital Hamiltonian population (COHP)[16] analysis, which is implemented in the TBLMTO-47 package.[17,18] A measure of the magnitude of bonding was obtained by computing COHP, which is the Hamilton population weighted density of states, identical to the well-known crystal-orbital-overlap population. In a simplified picture, negative COHP indicates a bonding character and positive, antibonding character. The bulk moduli have been obtained using the so-called universal-equation-of-state fit for total energy as a function of the volume.

Results and Discussion

For our simulations, we have chosen seven different possible closely related structure types, they are α-LiAlH$_4$ (monoclinic; $P2_1/c$),[19] α-NaAlH$_4$ (tetragonal; $I4_1/a$),[20] β-LiBH$_4$ (hexagonal; $P6_3mc$),[21] α-NaGaH$_4$ (orthorhombic; $Cmcm$),[22] NaBH$_4$ (cubic, $F\bar{4}3m$),[23] SrMgH$_4$ (orthorhombic; $Cmc2_1$),[24] and α-KGaH$_4$ (orthorhombic; $Pnma$).[25] In our previous communications on LiAlH$_4$,[26] NaAlH$_4$,[27] and KAlH$_4$,[28] we have reported on successful reproduction of the ground-state structures and prediction of new high-pressure modifications of LiAlH$_4$ and NaAlH$_4$. In this work, we present the ground-state structures for the remaining seven compounds in the ABH$_4$ series. We have also identified potential high-pressure phases for some of these compounds, but these aspects will be accounted for in a forthcoming paper. To identify the equilibrium structure of the ABH$_4$
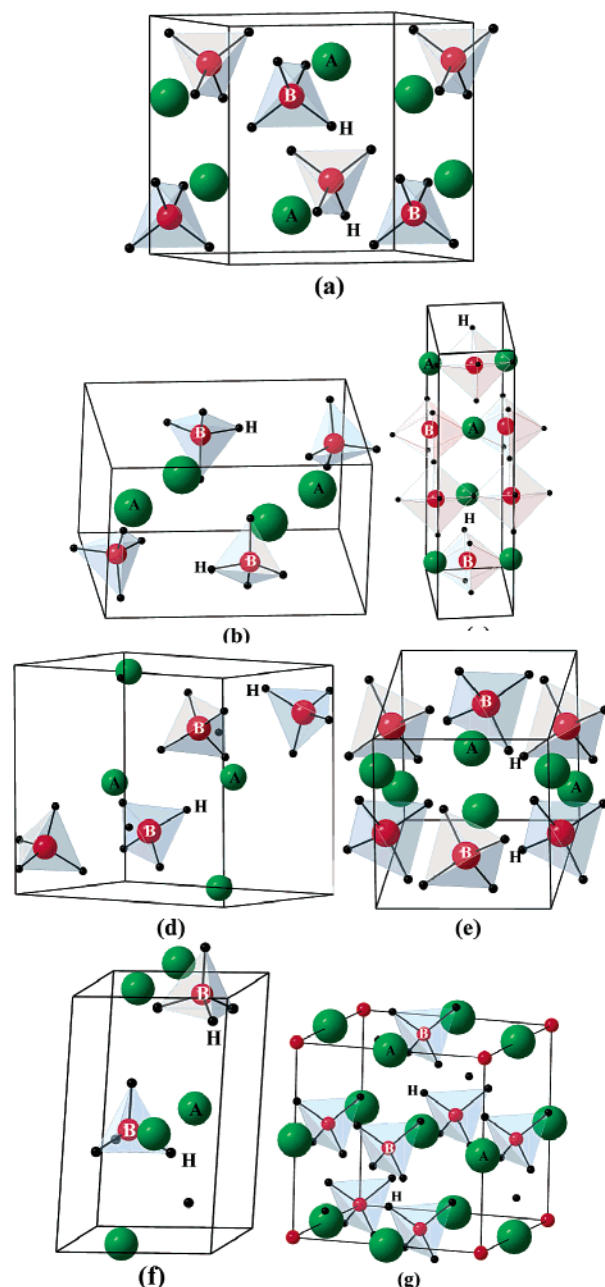
Figure 1. Crystal structure of ABH_4 in possible different structural arrangements [(a) $NaGaH_4$ (orthorhombic; *Cmcm*), (b) $KGaH_4$ (orthorhombic; *Pnma*), (c) $SrMgH_4$ (orthorhombic; *Cmc2$_1$*), (d) $LiAlH_4$ (monoclinic; *P2$_1$/c*), (e) α-$NaAlH_4$ (tetragonal; *I4$_1$/a*), (f) β-$LiBH_4$ (hexagonal; *P6$_3$mc*), and (g) $NaBH_4$ (cubic; *F$\bar{4}$3m*)].

phases, we have adopted the following procedure. First, for each trial structure, we have optimized the atomic coordinates and cell parameters globally using stress and force mimization, and thus identified the optimized cell volume, atomic coordinates, and unit-cell dimensions. In the following step, we varied the unit-cell volume between −25 and +15% in steps of 5% and relaxed all atom coordinates and unit-cell dimensions globally for each volume. The resulting cell volume vs free-energy relations for the considered possible structural arrangements for $KGaH_4$ are illustrated in Figure 2. The equilibrium volumes and bulk moduli were extracted from the calculated energy vs cell volume data by fitting them to the "universal equation of state"
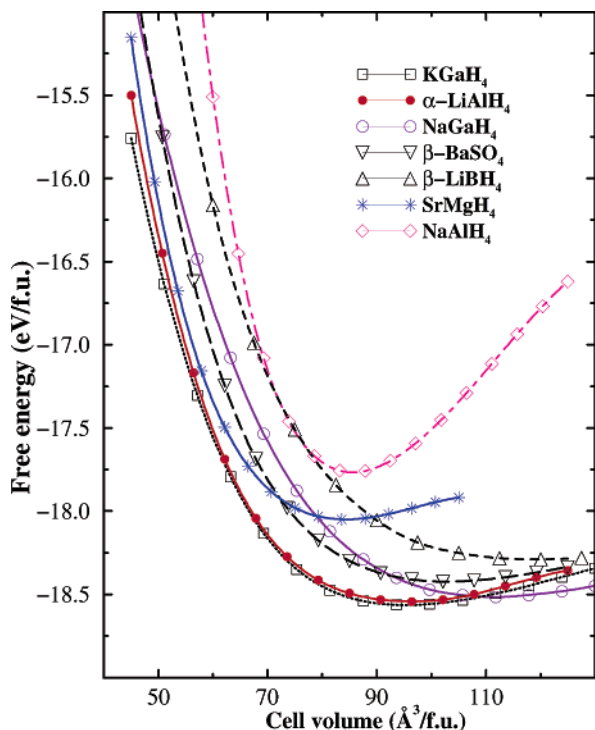
Figure 2. Calculated cell volume vs free energy curves for KGaH$_4$ in different possible arrangements (indicated on the illustration).

Figure 3. Variation in the cell volume along the ABH$_4$ series.

proposed by Vinet et al.[32] (virtually the same results were obtained by fitting to the Birch[33] or Murnaghan[34] equation).

From the total-energy minimization procedure, we have extracted the equilibrium structure parameters. In good agreement with the experimental findings for KGaH$_4$, the orthorhombic prototype structure takes the lowest energy (see Figure 2) with cell parameters in good agreement with the experimental[25] findings (see Table 1). In addition to the experimentally known prototype structure, a variant with α-LiAlH$_4$-type structure also exists close in energy (estimated energy difference only 0.02 eV/f.u.). Both structures have almost similar equilibrium volume (95.62 and 96.43 Å^3/f.u. for the KGaH$_4$ and α-LiAlH$_4$ type, respectively). This indicates that syntheses under appropriate pressure and temperature conditions may be able to generate the α-LiAlH$_4$-type arrangement as a metastable state. Similarly, for the other known compounds in the series, experimentally identified structures (α-LiAlH$_4$, -NaAlH$_4$, and -NaGaH$_4$) proved to have the lowest energy among the considered alternatives. The good agreement (1–2% in unit-cell dimensions) between experimental and calculated structure data (Table 1) demonstrates the reliability of the calculation and lends confidence to the structural data extracted for the hitherto unknown members of the series (remembering that our calculations refer to 0 K, viz. temperature effects are not taken into account). From the total-energy-minimization procedure, we have found that KAlH$_4$, RbAlH$_4$, CsAlH$_4$, RbGaH$_4$, and CsGaH$_4$ stabilize in the KGaH$_4$-type structure (see Table 1), and the following discussion is valid only for these isostructural phases. In the KGaH$_4$-type structure, the B atoms are tetrahedrally coordinated to four hydrogen atoms that are in three crystal-lographically different positions. The [BH$_4$] (anion) tetrahedra (which are slightly distorted) are kept apart by the A (here A = K, Rb, Cs) cations. The average B–H separations within the [BH$_4$]$^-$ tetrahedra vary from 1.602 (RbGaH$_4$) to 1.645 Å (KAlH$_4$) (two B–H distances of one kind and two others of a different kind). Each A$^+$ is surrounded by 12 H atoms, with A–H distances varying between 2.689 (KAlH$_4$) and 3.092 Å (CsAlH$_4$).
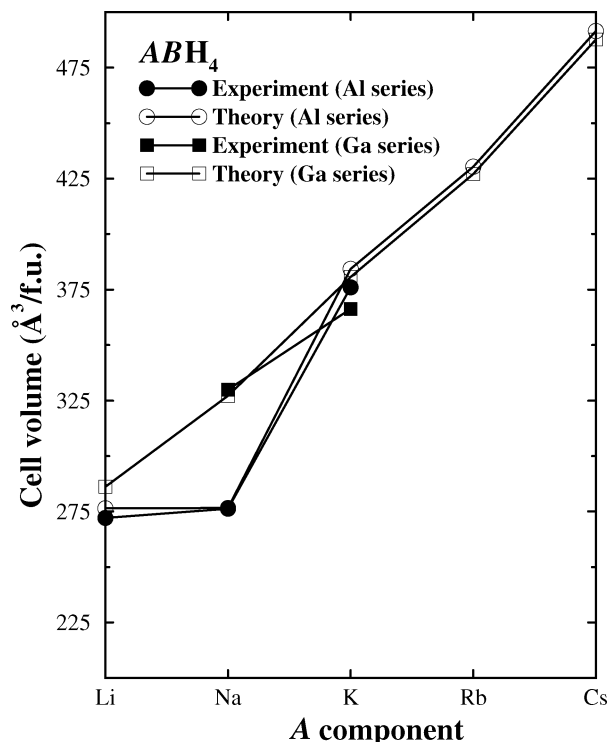
Among the 10 considered phases KAlH$_4$, RbAlH$_4$, CsAlH$_4$, KGaH$_4$, RbGaH$_4$, and CsGaH$_4$ are isostructural, whereas LiAlH$_4$, NaAlH$_4$, and NaGaH$_4$ take different structural arrangements. On going from A = Li to Cs in the Ga-based compounds, the calculated equilibrium volumes vary almost linearly (Figure 3). This concurs with the fact that on moving downward on the periodic table the atomic radii increases roughly linearly, a behavior reflected in the cell volumes. On the other hand, among the Al-based compounds, the cell volume of NaAlH$_4$ deviates from a linear pattern in that LiAlH$_4$ and NaAlH$_4$ have almost similar equilibrium volume (276.41 and 276.68 Å^3, respectively).

The preference for different packing among the ABH$_4$ series can readily be rationalized by their ionic radii (0.59, 0.97, 1.37, 1.52, and 1.67 Å for Li, Na, K, Rb, and Cs, respectively). A common feature for the series is the comparatively large [BH$_4$]$^-$ building block and its size determining influence of the overall structures. The interatomic B–H distance within the [BH$_4$]$^-$ unit is almost the same (running between 1.60 and 1.64 Å; shortest in the AGaH$_4$ series largest for KAlH$_4$). On moving from Li to Cs in these series, the calculated A–H distance varies linearly and the H–H separation increases from 2.56 to 2.71 Å. In LiAlH$_4$, the large [AlH$_4$]$^-$ anion tends to adopt hexagonal close packing, which would minimize the hole size for the small Li$^+$ cation (the monoclinic β angle is ~112°, viz. close to the hexagonal β = 120°).

Table 1. Optimized Structural Parameters, Bulk Modulus (B_0), and Its Pressure Derivative (B_0') for ABH$_4$ Compounds

compound	unit-cell dimensions (Å)	atomic positions	B_0 (GPa)	B_0'
α-LiAlH$_4$ (prototype; $P2_1/c$)	$a = 4.8535\ (4.8174)^a$ $b = 7.8259\ (7.8020)^a$ $c = 7.8419\ (7.8214)^a$ $\beta = 111.878\ (112.228)^a$	Li(4e): 0.5699, 0.4652, 0.8245 (0.5603, 0.4656, 0.8266)^a Al(4e): 0.1381, 0.2017, 0.9319 (0.1386, 0.2033, 0.9302)^a H1(4e): 0.1807, 0.0986, 0.7630 (0.1826, 0.0958, 0.7630)^a H2(4e): 0.3542, 0.3723, 0.9777 (0.3524, 0.3713, 0.9749)^a H3(4e): 0.2361, 0.0810, 0.1146 (0.2425, 0.0806, 0.1148)^a H4(4e): 0.7948, 0.2633, 0.8717 (0.7994, 0.2649, 0.8724)^a	12.95	4.10
α-NaAlH$_4$ (proto-type; $I4_1/a$)	$a = 4.9965\ (4.9801)^b$ $c = 11.0828\ (11.1483)^b$	Na(4a): 0, 1/4, 1/8 Al(4b): 0, 1/4, 5/8 H(16f): 0.2299, 0.3710, 0.5639 (0.2372, 0.3869, 0.5456)^b	19.31	4.77
KAlH$_4$ (KGaH$_4$-type; $Pnma$)	$a = 8.950\ (8.814)^c$ $b = 5.803\ (5.819)^c$ $c = 7.394\ (7.331)^c$	K(4c): 0.1778, 1/4, 0.1621 Al(4c): 0.5663, 1/4, 0.8184 H1(4c): 0.4034, 1/4, 0.9184 H2(4c): 0.7055, 1/4, 0.9623 H3(8d): 0.4194, 0.9810, 0.3127	10.34	4.61
α-RbAlH$_4$ (KGaH$_4$-type; $Pnma$)	$a = 9.5956$ $b = 5.7662$ $c = 7.7795$	Rb(4c): 0.1823, 1/4, 0.1597 Al(4c): 0.5615, 1/4, 0.8138 H1(4c): 0.4017, 1/4, 0.8990 H2(4c): 0.6883, 1/4, 0.9610 H3(8d): 0.4198, 0.9762, 0.3121	9.22	4.94
α-CsAlH$_4$ (KGaH$_4$-type; $Pnma$)	$a = 10.0520$ $b = 6.0945$ $c = 8.0232$	Cs(4c): 0.1868, 1/4, 0.1580 Al(4c): 0.5570, 1/4, 0.8078 H1(4c): 0.4034, 1/4, 0.8847 H2(4c): 0.6741, 1/4, 0.9541 H3(8d): 0.4226, 0.9708, 0.3127	8.35	5.42
α-LiGaH$_4$ (NaGaH$_4$-type; $Cmcm$)	$a = 6.5275$ $b = 7.0384$ $c = 6.2093$	Li(4c): 0, 0.4260, 1/4 Ga(4c): 0, −0.1783, 1/4 H(8f): 0, 0.6740, 0.4536 H(8g): 0.1799, −0.0486, 1/4	11.97	5.04
α-NaGaH$_4$ (proto-type; $Cmcm$)	$a = 7.1102\ (7.07)^d$ $b = 6.4717\ (6.60)^d$ $c = 7.1089\ (7.06)^d$	Na(4c): 0, 0.3439, 1/4 (0, 0.3370, 1/4)^d Ga(4c): 0, −0.1599, 1/4 (0, −0.166, 1/4)^d H1(8f): 0, 0.6879, 0.4313 (0, 0.6960, 0.4260)^d H2(8g): 0.1409, −0.0109, 1/4 (0.1630, −0.0380, 1/4)^d	13.19	4.93
KGaH$_4$ (proto-type; $Pnma$)	$a = 9.1133\ (8.987)^e$ $b = 5.6467\ (5.613)^e$ $c = 7.3990\ (7.262)^e$	K(4c): 0.1806, 1/4, 0.1616 (0.1886, 1/4, 0.1537)^e Ga(4c): 0.5632, 1/4, 0.8096 (0.5689, 1/4, 0.8110)^e H1(4c): 0.3990, 1/4, 0.8951 (0.4133, 1/4, 0.8864)^e H2(4c): 0.6939, 1/4, 0.9620 (0.6805, 1/4, 0.9641)^e H3(8d): 0.4119, 0.9862, 0.3197 (0.4224, 0.9737, 0.3108)^e	10.15	4.95
α-RbGaH$_4$ (KGaH$_4$-type; $Pnma$)	$a = 9.5390$ $b = 5.8275$ $c = 7.6823$	Rb(4c): 0.1781, 1/4, 0.1689 Ga(4c): 0.5681, 1/4, 0.8095 H1(4c): 0.4112, 1/4, 0.9122 H2(4c): 0.7081, 1/4, 0.9483 H3(8d): 0.4165, 0.9810, 0.3231	9.41	5.06
α-CsGaH$_4$ (KGaH$_4$-type; $Pnma$)	$a = 10.0154$ $b = 6.0995$ $c = 7.9831$	Cs(4c): 0.1794, 1/4, 0.1653 Ga(4c): 0.5652, 1/4, 0.8076 H1(4c): 0.4025, 1/4, 0.8970 H2(4c): 0.6994, 1/4, 0.9526 H3(8d): 0.4163, 0.9796, 0.3229	8.22	5.20

^{a} From ref 19. ^{b} From ref 29. ^{c} From ref 30. ^{d} From ref 31. ^{e} From ref 25.

Experimental values for bulk modulus are not available for these compounds, and hence theoretical predications of B_0 are of interest. A relationship between binding energy and interatomic distances has been discovered for so-called bimetallic adhesion,[35] chemisorption on metals,[36] and metallic cohesion.[37] Vinet et al.[32] proposed a universal equation of state (UEOS) for all classes of solids in compression, which is claimed to be superior to that of the Birch−Murnaghan EOS.[34] The calculated bulk modulus varies almost linearly along the series (Table 1; except for NaAlH$_4$) viz. consistent with the volume variation in this series. The maximum values of B_0 for NaAlH$_4$ suggest that enhanced bond strength for this compound may be the cause of the dip in the cell volume relations. The magnitude of B_0 classifies these ABH$_4$ compounds as easily compressible materials (the B_0 values in Table 1 being about 3 times smaller than for MgH$_2$).

Density of States (DOS). The total DOS for ABH$_4$ shows close similarities (data for the AGaH$_4$ series being reported in Figure 4). The partial density of states (PDOS) is a useful tool to analyze the nature of the chemical bonding in solids;[38] hence we display PDOS curves for KGaH$_4$ in Figure 5. In general, these ABH$_4$ compounds have a finite energy gap between the valence and conduction bands, and accordingly they exhibit nonmetallic features. The total DOS (Figure 4) for the AGaH$_4$ phases comprises three well-separated regions; region I: below −5 eV, region II: from −3 to 0 eV, and region III: above 5 eV (unoccupied states). On going from LiGaH$_4$ to CsGaH$_4$, the width of the bands (in particular the VB; see Figure 5) is narrowed. Recalling that the Ga−H distance does not vary much along the AGaH$_4$ series it seems safe to conclude that it is the enhancement in the A−H interaction which is the main reason for the reduction in the VB width.

From an electronegativity point of view, the bonding B−H interaction should be of a covalent nature, whereas the A−H interaction should be ionic. Looking at the site projected DOS of K and Ga (middle panels of Figure 5),
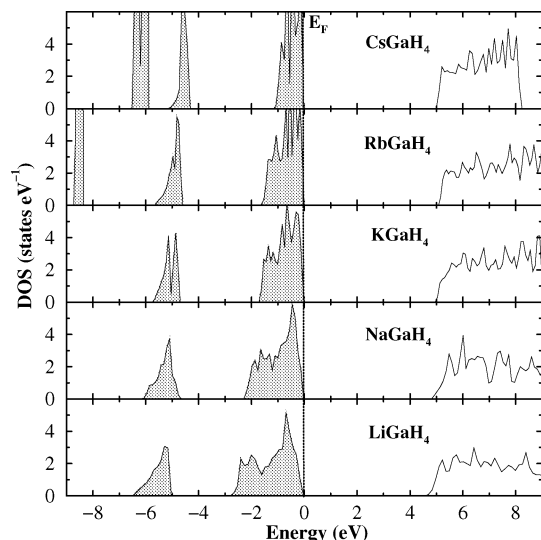
Figure 4. Calculated total density of states for $AGaH_4$ compounds. The Fermi level is set at zero energy and marked by vertical lines.
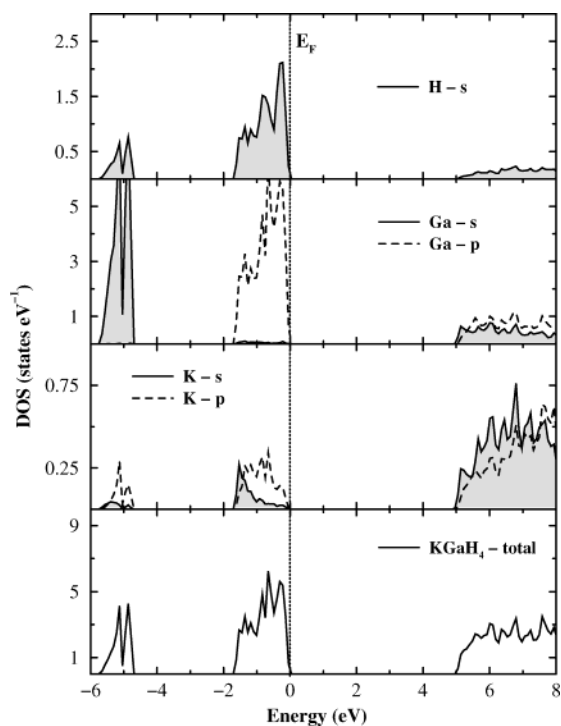
Figure 5. Calculated partial density of states for $KGaH_4$. The Fermi level is set at zero energy and marked by vertical dotted lines; *s*-electron contributions are depicted in gray.

the region I is mainly originating from Ga-*s* states with only small contribution from K-*s* and -*p* states. Region II is mainly contributed by Ga-*p*, K-*s* and -*p*, and H-*s* states. Ga-*s* and -*p* states are energetically well separated in the VB region, whereas K-*s* and -*p* states are energetically degenerate. The degeneration of Ga-*p* and H-*s* states in the VB region reflects the elementary text book picture of sp^3 hybridation in a tetrahedral unit like $[GaH_4]$ (with a spatially favorable situation for such hybridized bonding). The calculated band gap (E_g) for these compounds varies from 4.5 to 5.5 eV, $LiGaH_4$ having the smallest and $KAlH_4$ the largest band gap. $RbAlH_4$, $KGaH_4$, $RbGaH_4$, and $CsGaH_4$ have $E_g \approx 5$ eV,

which may reflect the isostructural charecter of these phases. The calculated E_g values are quite close to that of other technologically important hydrides[15] like MgH_2 (4.3 eV). It should be recalled that theoretically derived band gaps in semiconductors and insulators may be underestimated by 20−50 using first-principle methods.[39]

Charge Density and Electron Localization Function. To get better insight into the chemical bonding in these compounds, we have made charge-density distribution and electron localization function (ELF) analyses. From an application point of view, such analyses may help to identify potential substitution elements that can improve the properties of such materials. Like DOS, the charge-density distribution and ELF show similar features for series such as this, and the following account will therefore be focused on $KGaH_4$.

Figure 6 shows the calculated valence-charge density (obtained directly from the self-consistent calculations) within the (101) plane. At the K, Ga, and H sites, it is clear that the highest charge density resides in the immediate vicinity of the nuclei. The predominant covalent nature of the bonding between Ga and H is further reconfirmed by the finite charge between these atoms. The H-*s* electrons are tightly bound to the Ga-*p* states, and the formation of sp^3 hybridization concurs with $[GaH_4]$ units in a K matrix (in support of the conclusions form DOS). The electron distribution between K and the $[GaH_4]$ unit is almost zero (charge depleted; see Figure 6), viz. an ionic type of interaction is present between $[GaH_4]$ and K.

ELF is a ground-state property that discriminates in a quantitative way between different kinds of bonding.[40,41,42] In the implementation for density-functional theory, this quantity depends on the excess of local kinetic energy due to the Pauli principle. In general, ELF becomes 1 either for single-electron or any two-electron singlet-wave function. In a many-electron system ELF becomes close to 1 in regions where electrons are paired to form a covalent bond, and also close to 1 for a region with an unpaired lone electron of a dangling bond. In a homogeneous electron gas ELF equals 0.5 at any electron density, values of this order indicating regions with bonding of a metallic character. The ELF value between Ga and H in $KGaH_4$ is 1, again consistent with covalent type of interaction between the Ga and H. Figure 7, right panel shows an ELF plot at an iso-surface value of 0.75, which further emphasizes the distribution of distinct $[GaH_4]$ units in a K matrix. The ELF value at the K site is ~0.2 and between the K site and the interstitial region ELF is virtually zero. The ELF findings thus reinforces the ionic bonding between K^+ and $[GaH_4]^-$ with strong covalent internal bonding within the latter units.

Crystal Orbital Hamilton Population Analysis. To evaluate the bond strength between the involved atoms, we have performed COHP analysis. Integrated COHP (ICOHP) up to E_F gives the magnitude of the bond strength and the result from such COHP analyses for $KGaH_4$ is shown in Figure 8 for all possible combinations of the involved constituents. The VB comprises mainly bonding orbitals (negative COHP), whereas antibonding orbitals are found some ~3.5 eV above E_F. The most notable feature in Figure 8 is the remarkable
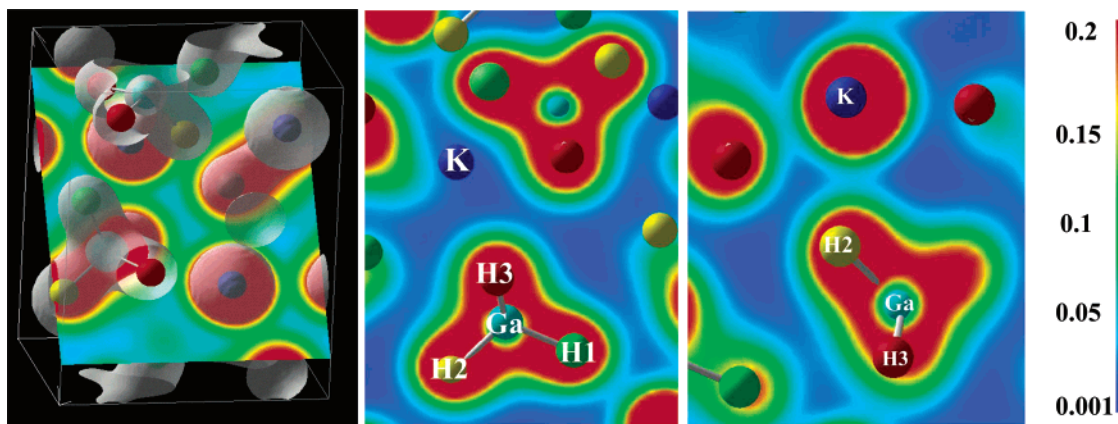
Figure 6. KGaH$_4$. Left panel: Calculated three-dimensional charge-density distribution. Middle panel: Charge-density distribution in the (1 0 1) plane. Right panel: To obtain a clearer view of the charge distribution at the K site, the origin is slightly shifted in the *z* direction (the structural segment shown being also changed). Color code gives the density scale.
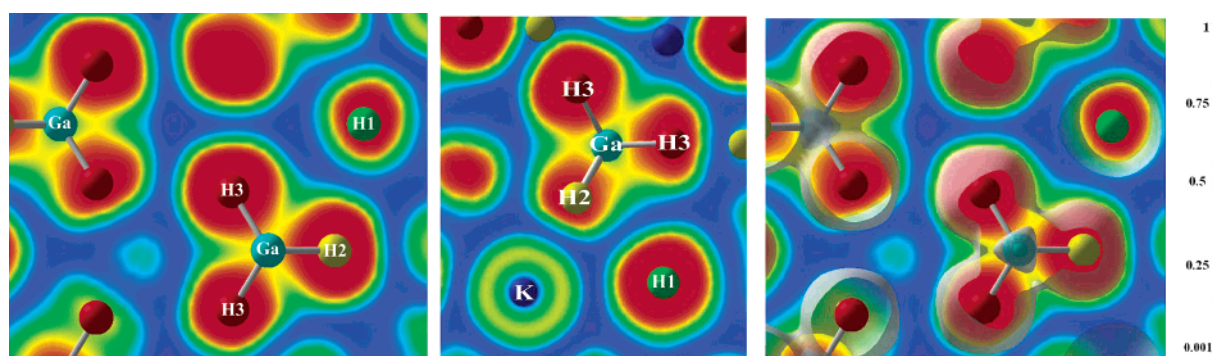
Figure 7. KGaH$_4$. Left panel: Calculated ELF plot in the (1 0 1) plane (between Ga, H1, H2, and H3 atoms). Middle panel: A slightly shifted origin in the *z* direction (between K, Ga, H1, H2 and H3 atoms; the structural segment shown being also changed) compared to the left panel. Right panel: ELF with isosurface value 0.75. The color code gives the density scale.

strength of the Ga−H interaction (−2.62 to −3.44 eV in ICOHP, similar for all B−H interactions in this series) compared to the other interactions. Moving from A = Li to Cs the B−H interaction (covalent bond strength) is reduced (both in the Al and Ga series) According to the calculated ICOHP for these compounds, the Al−H bond is stronger than the Ga−H bond. This indicates that the stability (and hence the decomposition temperature) in the Al series is higher than in the Ga series. It implies that the partial substitution of Li by other alkaline elements in materials such as Li$_{1-x}$Na$_x$AlH$_4$, Li$_{1-x}$K$_x$AlH$_4$, or Li$_{1-x}$K$_x$Al$_{1-y}$Ga$_y$H$_4$ may give lower decomposition temperatures.

In addition to the B−H interaction, the A−H (−0.31 to −0.43 eV) and A−B (−0.09 to −0.12 eV) interactions also have considerable ICOHP values in these ABH$_4$ compounds, however, appreciably smaller than the B−H interactions. The ICOHP for H1−H2 up to E_F has an almost negligible value, which perhaps indicates the presence of both bonding and antibonding states in this interaction. Thus with both bonding and antibonding states present in almost equal amounts in the VB region the covalent interaction between the hydrogen atoms will not contribute significantly to the stability of these systems. It implies that the B−H interaction is the main cause for the relatively high decomposition temperature of these phases.

Conclusion

The crystal structure of an entire series of ABH$_4$ compounds have been investigated from first-principle density-functional calculations for different possible structural modifications. The calculated atomic position and cell parameters are in very good agreement with experimental findings for LiAlH$_4$, NaAlH$_4$, KAlH$_4$, NaGaH$_4$, and KGaH$_4$. The crystal structure for RbAlH$_4$, CsAlH$_4$, LiGaH$_4$, RbGaH$_4$, and CsGaH$_4$ are predicted. The values of calculated bulk modulus indicate that all these materials should be easily compressible. A density of states examination shows that these compounds have a nonmetallic nature and with calculated band gaps around 5 eV. The calculated Al−H and Ga−H distances are almost the same for all compounds, implying that all of these compounds have almost the same size of the [BH$_4$]$^-$ structural units. From the partial DOS, charge density, and ELF study, it is concluded that these compounds are ionic materials with covalent interaction between B and H in the [BH$_4$]$^-$ units and ionic between the [BH$_4$]$^-$ and A$^+$. From the COHP analysis, we have identified that the magnitude of the B−H interaction is stronger than the other interactions in these compounds. The Al(Ga)−H bond strength is reduced when we move from the top to the bottom of the alkali metals in the periodic table. This suggests that substitution of
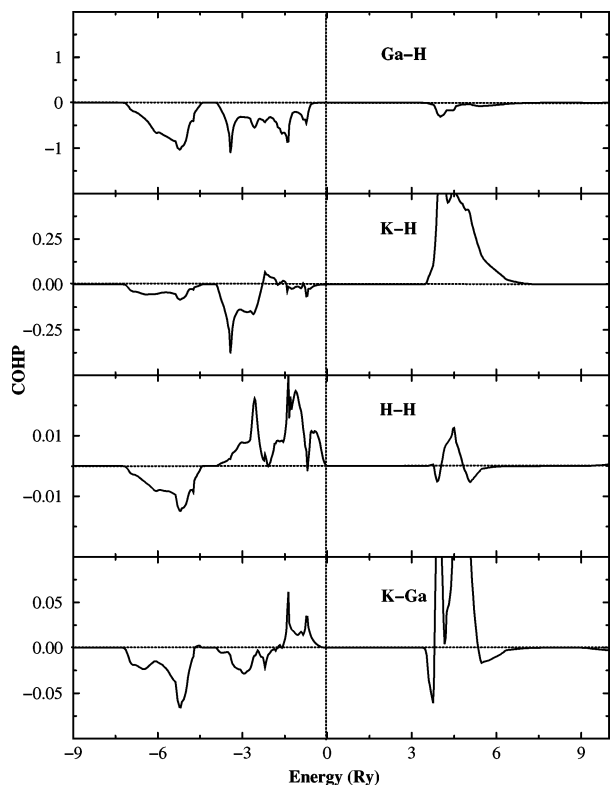
Figure 8. COHP curves for KGaH₄; referring to the combinations Ga−H1, K−H1, H1−H2, and K−Ga.

Li by an other alkali elements in LiAlH₄ may reduce the decomposition temperature.

References

(1) Yvon, K. *Encyclopedia of Inorganic Chemistry*; King, R. B., Ed.; Wiley: New York, 1994; Vol. 3, p 1401.
(2) Buschow, K. H. J.; Van Mall, H. H.; Googwell, P. D.; Rudman, P. S. *J. Less-Common Met.* **1972**, *29*, 203.
(3) Reilly, J. J.; Wiswall, R. H. *Inorg. Chem.* **1974**, *13*, 218.
(4) Bogdanovic, B.; Schwickardi, M. *J. Alloys Compd.* **1997**, *253−254*, 1.
(5) Block, J.; Gray, A. P. *Inorg. Chem.* **1965**, *4*, 304.
(6) Dilts, J. A.; Ashby, E. C. *Inorg. Chem.* **1972**, *11*, 1230; Bastide, J. P.; Monnetot, B.; Letoffe, J. M.; Claudy, P. *Mater. Res. Bull.* **1985**, *20*, 997.
(7) Bogdanovic, B.; Brand, R. A.; Marjanovic, A.; Schwikardi, M.; Tölle, J. *J. Alloys Compd.* **2000**, *302*, 36.
(8) Brinks, H. W.; Hauback, B. C.; Norby, P.; Fjellvåg, H. *J. Alloys Compd.* **2003**, *315*, 222.
(9) Jensen, C. M.; Gross, K. *J. Appl. Phys. A* **2001**, *72*, 213.
(10) Morioka, H.; Kakizaki, K.; Chung, S. C.; Yamada, A. *J. Alloys Compd.* **2003**, *353*, 310.
(11) Hohenberg, P.; Kohn, W. *Phys. Rev.* **1964**, *136*, 864B.
(12) Perdew, J. P. *Electronic Structure of Solids*; Ziesche, P.; Eschrig, H., Eds.; Akademie Verlag: Berlin, 1991; p 11; Perdew, J. P.; Burke, K.; Wang, Y. *Phys. Rev. B* **1996**, *54*, 16533; Perdew, J. P.; Burke, K.; Ernzerhof, M. *Phys. Rev. Lett.* **1996**, *77*, 3865.
(13) Kresse, G.; Hafner, J. *Phys. Rev. B* **1993**, *47*, R6726; Kresse, G.; Furthmuller, J. *Comput. Mater. Sci.* **1996**, *6*, 15.
(14) Blöchl, P. E. *Phys. Rev. B* **1994**, *50*, 17953; Kresse, G.; Joubert, J. *Phys. Rev. B*, **1999**, *59*, 1758.
(15) Vajeeston, P.; Ravindran, P.; Kjekshus, A.; Fjellvåg, H. *Phys. Rev. Lett.* **2002**, *89*, 175506.
(16) Dronskowski, R.; Blochl, P. E. *J. Phys. Chem. B* **1993**, *97*, 8617.
(17) Andersen, O. K. *Phys. Rev. B* **1975**, *12*, 3060; Andersen, O. K.; Jepsen, O. *Phys. Rev. B* **1984**, *53*, 2571; Skriver, H. L. *The LMTO Method*; Springer: Heidelberg, Germany, 1984.
(18) Krier, G.; Jepsen, O.; Burkhardt, A.; Andersen, O. K. Tight Binding LMTO-ASA Program, Version 4.7, Stuttgart, Germany, 2000.
(19) Hauback, B. C.; Brinks, H. W.; Fjellvåg, H. *J. Alloys Compd.* **2002**, *346*, 184.
(20) Belskii, V. K.; Bulychev, B. M.; Golubeva, A. V. *Acta Crystallogr., Sect. B: Struct. Sci.* **1982**, *38*, 1254.
(21) Soulié, J. P.; Renaudin, G.; Eerny, R.; Yvon, K. *J. Alloys Compd.* **2002**, *346*, 200.
(22) Irodova, A. V.; Somenkov, V. A.; Kurchatovy, I. V.; Bakum, S. I.; Kuznetsova, S. F.; Kurnakov, N. S. *Z. Phys. Chem.* **1989**, *163*, 239.
(23) Davis, R. L.; Kennardy, C. H. L. *J. Solid State Chem.* **1985**, *59*, 393.
(24) Gingl, F.; Yvon, K.; Fischer, P. *J. Alloys Compd.* **1992**, *187*, 105.
(25) Backum, S. I.; Irodova, A. V.; Kuznetsova, S. F.; Lyakhovitskaya, O. I.; Nozik, Y. Z.; Somenkov, V. A. *Russ. J. Coord. Chem.* **1990**, *16*, 1210.
(26) Vajeeston, P.; Ravindran, P.; Kjekshus, A.; Fjellvåg, H. *Phys. Rev. B.* **2003**, *68*, 212101.
(27) Vajeeston, P.; Ravindran, P.; Vidya, R.; Kjekshus, A.; Fjellvåg, H. *Appl. Phys. Lett.* **2003**, *82*, 2257.
(28) Vajeeston, P.; Ravindran, P.; Kjekshus, A.; Fjellvåg, H. *J. Alloys Compd.* **2003**, *363*, L8.
(29) Hauback, B. C.; Brinks, H. W.; Jensen, C. M.; Maeland, A. J. *J. Alloys Compd.* **2003**, *358*, 142.
(30) Bastide, J. P.; Claudy, P.; Letoffe, J. M.; Hajri, J. E. *Rev. Chim. Mineral.* **1987**, *24*, 248.
(31) Irodova, A. V.; Somenkov, V. A.; Kurchatov, I. V.; Bakum, S. I.; Kunznetsova, S. F.; Kurnakov, N. S. *Z. Phys. Chem.* **1989**, *163*, 239.
(32) Vinet, P.; Ferrante, J.; Smith, J. R.; Rose, J. H. *J. Phys. C* **1986**, *19*, L467; Vinet, P.; Rose, J. H.; Ferrante, H.; Smith, J. R. *J. Phys.: Condens. Matter* **1989**, *1*, 1941.
(33) Birch, F. *Phys. Rev.* **1947**, *71*, 809.
(34) Murnaghan, F. D. *Proc. Natl. Acad. Sci. U.S.A.* **1944**, *30*, 244.
(35) Rose, J. H.; Ferrante, J.; Smith, J. R. *Phys. Rev. Lett.* **1981**, *47*, 675.
(36) Smith, J. R.; Ferrante, J.; Rose, J. H. *Phys. Rev. B* **1985**, *31*, 3427.
(37) Ferrante, J.; Smith, J. R.; Rose, J. H. *Phys. Rev. B* **1983**, *28*, 1835.
(38) Gelatt, C. D.; Williams, A. R.; Maruzzi, V. L. *Phys. Rev. B* **1983**, *27*, 2005.
(39) *Theory of the Inhomogeneous Electron Gas*; Lundqvist, S., March, N. H., Eds.; Plenum: New York, 1983.
(40) Savin, A.; Becke, A. D.; Flad, J.; Nesper, R.; Preuss, H.; Schnering, H. G. *Angew. Chem., Int. Ed. Engl.* **1991**, *30*, 409; Savin, A.; Jepsen, O.; Flad, J.; Andersen, O. K.; Preuss, H.; Schnering, H. G. *Angew. Chem., Int. Ed. Engl.* **1992**, *31*, 187.
(41) Silvi, B.; Savin, A. *Nature* **1994**, *371*, 683.
(42) Becke, A. D.; Edgecombe, K. E. *J. Chem. Phys.* **1990**, *92*, 5397.